Comparison of the RGD Motif–Containing $\alpha_v\beta_6$ Integrin–Binding Peptides SFLAP3 and SFITGv6 for Diagnostic Application in HNSCC

Saskia Roesch*[1,2], Thomas Lindner*[3], Max Sauter*[3,4], Anastasia Loktev[5], Paul Flechsig[6], Martin Müller[5], Walter Mier[3], Rolf Warta[1,2], Gerhard Dyckhoff[1], Christel Herold-Mende[1,2], Uwe Haberkorn[3,5], and Annette Altmann[3,5]

[1]*Department of Otorhinolaryngology, University Hospital Heidelberg, Heidelberg, Germany;* [2]*Division of Experimental Neurosurgery, Department of Neurosurgery, University Hospital Heidelberg, Heidelberg, Germany;* [3]*Department of Nuclear Medicine, University Hospital Heidelberg, Heidelberg, Germany;* [4]*Department of Clinical Pharmacology and Pharmacoepidemiology, University Hospital Heidelberg, Heidelberg, Germany;* [5]*Clinical Cooperation Unit Nuclear Medicine, German Cancer Research Center (DKFZ), Heidelberg, Germany; and* [6]*Department of Radiology, University Hospital Heidelberg, Heidelberg, Germany*

$\alpha_v\beta_6$ integrin is overexpressed by several carcinomas and thus considered a target for diagnostic imaging and anticancer therapies. Recently, we presented the $\alpha_v\beta_6$ integrin-binding peptide SFITGv6 as a novel potential tracer for imaging and targeted therapy of $\alpha_v\beta_6$ integrin–positive carcinomas. Here, we analyzed the affinity and specificity of 5 native $\alpha_v\beta_6$ integrin–specific binders in comparison to SFITGv6. **Methods:** Sunflower trypsin inhibitor 1 (SFTI1)–based peptides containing arginine-glycine-aspartic acid (RGD) motif-spanning octamers of fibronectin (SFFN1), tenascin C (SFTNC), vitronectin (SFVTN), and latency-associated peptides (LAP) 1 (SFLAP1) and 3 (SFLAP3) were synthesized, and their binding potential to $\alpha_v\beta_6$ integrin–expressing head and neck squamous cell carcinoma (HNSCC) cell lines was evaluated. Subsequently, stability, affinity, and specificity were assessed in vitro using radio–high-pressure liquid chromatography, surface plasmon resonance assay, and binding experiments including competition, kinetics, internalization, and efflux. $\alpha_v\beta_6$ integrin binding specificity was further evaluated by peptide histochemistry. Finally, in vivo binding properties were assessed using small-animal PET imaging and biodistribution experiments in HNSCC-bearing mice, and ^{68}Ga-DOTA-SFLAP3 was applied for diagnostic PET/CT of an HNSCC patient. **Results:** When the newly designed peptides were compared, significant binding (>20%) to several HNSCC cell lines (HNO97, HNO399, and HNO223) and a fast internalization of up to 60% and 70% were observed for SFLAP3 (GRGDLGRL) and SFITGv6 (FRGDLMQL). In contrast, the other peptides displayed binding that was moderate (SFLAP1, 4.1%–12.1%) to marginal (SFFN1, SFTNC, and SFVTN, <1%) and were therefore excluded from further analysis. Notably, SFLAP3 exhibited improved affinity for $\alpha_v\beta_6$ integrin (mean half-maximal inhibitory concentration, 3.5 nM; dissociation constant, 7.4). Moreover, small-animal PET imaging and biodistribution studies of HNSCC xenograft mice revealed an increased tumor-specific accumulation 30–60 min after injection of ^{68}Ga-labeled or ^{177}Lu-labeled DOTA-SFLAP3. Peptide staining further demonstrated binding specificity for SFLAP3 to HNSCC tumor cells. Finally, PET/CT scanning of an HNSCC patient showed specific SFLAP3 accumulation in the primary tumor lesion (SUV_{max}, 5.1) and in corresponding lymph node metastases (SUV_{max}, 4.1). **Conclusion:** SFLAP3 represents a promising tracer for prognostic assessment, diagnostic imaging, and possibly targeted therapy of $\alpha_v\beta_6$ integrin–expressing tumors.

Key Words: $\alpha_v\beta_6$; integrin; novel peptide; head and neck squamous cell carcinoma; PET

J Nucl Med 2018; 59:1679–1685
DOI: 10.2967/jnumed.118.210013

Integrins comprise a large family of cellular adhesion receptors that play an important role in development, immune response, and cancer (*1–3*). Unlike most epithelial integrins, $\alpha_v\beta_6$ integrin is upregulated in many carcinomas associated with a poor prognosis, including lung, ovarian, pancreatic, colorectal, and cervical (*4–8*). In contrast, healthy tissues show no or a rather low $\alpha_v\beta_6$ integrin expression (*9*). Therefore, $\alpha_v\beta_6$ integrin is considered a prognostic biomarker and an important target for imaging and anticancer therapies (*10,11*). Using a sunflower trypsin inhibitor 1 (SFTI1)–based phage display library for biopanning against head and neck squamous cell carcinoma (HNSCC) cells and fractionated high-pressure liquid chromatography–derived membrane proteins, we identified the novel $\alpha_v\beta_6$ integrin–specific peptide SFITGv6 (*12*). Because of the molecular scaffold of SFTI1, a 14-residue cyclic miniprotein isolated from sunflower seeds that is stabilized by a single disulfide bridge, the peptide exhibits excellent stability (*13*). SFITGv6 demonstrates high binding affinity to several $\alpha_v\beta_6$ integrin–positive tumor cells and to HNSCC xenografts. Moreover, it accumulates in tumor lesions of HNSCC and non–small cell lung carcinoma but not in inflammatory lesions of cancer patients (*12*).

$\alpha_v\beta_6$ integrin binds the tripeptide recognition sequence arginine-glycine-aspartic acid (RGD) of several extracellular matrix proteins, including fibronectin, vitronectin, tenascin C, and latency-associated peptides (LAP) 1 and 3, which participate in carcinogenesis by promoting cell migration and invasion of cancer cells (14,15). Particularly, $\alpha_v\beta_6$ integrin–mediated transforming growth factor β (TGF-β) activation plays an important role in epithelial-to-mesenchymal transition and thereby promotes tumor growth and metastasis (16). Noncovalently associated with the N terminus of TGF-β1 and TGF-β3,

Received Feb. 15, 2018; revision accepted Mar. 28, 2018.
For correspondence or reprints contact: Annette Altmann, Department of Nuclear Medicine, University Hospital Heidelberg, INF400, 69120 Heidelberg, Germany.
E-mail: a.altmann@dkfz.de
*Contributed equally to this work.
Published online Apr. 19, 2018.

LAP prevents TGF-β from binding to TGF-β receptors. Binding of LAP1 or LAP3 to $\alpha_v\beta_6$ integrin induces dissociation of the complex followed by TGF-β activation (17,18). Considering both the requirement for additional tumor-specific peptides targeting epithelial tumors and the high stability of the SFTI1 scaffold (13), we designed further RGD sequence–containing SFTI1 derivates (SFTI1-based peptides containing RGD motif–spanning octamers of fibronectin [SFFN1], tenascin C [SFTNC], vitronectin [SFVTN], LAP1 [SFLAP1], and LAP3 [SFLAP3]) and compared their $\alpha_v\beta_6$ integrin–specific binding properties with those of SFITGv6. Thus, we discovered SFLAP3, a peptide that demonstrates high $\alpha_v\beta_6$ integrin affinity and specificity for several $\alpha_v\beta_6$ integrin–expressing tumor cells. Moreover, SFLAP3 displays an increased accumulation in HNSCC xenografts and patient tumors.

MATERIALS AND METHODS

Cell Lines, Tumor Material, and Ethical Approval

The HNSCC-derived cell lines HNO97, HNO199, HNO210, HNO223, and HNO399 (*19*) were cultured in RPMI 1640 medium supplemented with 10% fetal calf serum at 37°C and 5% CO_2 and were negative for *Mycoplasma* contamination. Uniqueness was assessed by the German Collection of Microorganisms and Cell Culture. Patient-derived tumor tissues obtained intraoperatively were snap-frozen and stored at −80°C. Written informed consent was obtained from all patients according to the research proposals approved by the Institutional Review Board at the Medical Faculty of the University of Heidelberg.

In Vitro Binding Experiments

For assessment of peptide binding capacity in vitro, $2.5–4 \times 10^5$ cells were seeded into 6-well plates and cultivated for 48 h. The cells were exposed to ^{125}I-labeled peptides resuspended in 1 mL of serum-free medium for 10 or 60 min either with or without different concentrations of unlabeled peptide (10^{-5}–10^{-10} M). Unbound peptide was washed off (3 washes with phosphate-buffered saline), and finally, cells were harvested using 0.3 M NaOH. To evaluate kinetic properties, the cells were exposed to ^{177}Lu-DOTA–labeled peptides for 10, 30, 60, 120, 360, and 480 min, respectively, and harvested using 0.3 M NaOH. Efflux was assessed by incubating the cells with ^{177}Lu-DOTA–labeled peptides for 60 min. Next, radioactive peptide-containing medium was replaced, and the cells were incubated for another 10, 30, 60, 120, and 240 min and finally harvested using 0.3 M NaOH. To assess peptide internalization, the cells were exposed to ^{177}Lu-DOTA–labeled peptides for 10, 30, 60, 120, and 240 min at 37°C. Surface-bound peptides were removed by 10 min of incubation with 1 M glycine-HCl solution (pH 2.2). The cells were rinsed with phosphate-buffered saline and lysed as described. Radioactivity (MBq) was determined using a γ-counter (LB951G; Berthold Technologies) and calculated as percentage of applied injected dose (%AD) per 10^6 cells.

Surface Plasmon Resonance Assay

Binding affinity was assessed via a BiaCore X100 system (GE Healthcare) as described in detail previously (*12*). Briefly, to prevent integrin heterodimer denaturation during immobilization, $\alpha_v\beta_6$ integrin (1, 2, 3, and 4 μg/mL) and $\alpha_v\beta_3$ integrin (15, 30, 35, and 40 μg/mL) were used as analytes. SFLAP3 was dissolved in HBS-EP (HEPES-buffered saline, containing EDTA and Surfactant P20) running buffer and immobilized (loading level, 12 response units) on the C1 sensor chip (both GE Healthcare) using a manual amine-coupling protocol. Next, the binding affinity of $\alpha_v\beta_6$ and $\alpha_v\beta_3$ integrin, dissolved in HBS-EP running buffer (1–50 μg/mL), to SFLAP3 was measured (flow rate, 30 μL/min). The dissociation constant (K_D) was determined by a 1:1 Langmuir model fit of the surface plasmon resonance sensograms.

Animal Experiments

Animal experiments were conducted in compliance with the German animal protection laws. For in vivo small-animal PET imaging and organ distribution studies, 8-wk-old BALB/c nude mice (Charles River Laboratories) were inoculated subcutaneously at the right shoulder with 5×10^6 tumor cells in Matrigel (BD Bioscience).

Xenografts were grown to a 10- to 15-mm diameter. The mice were anesthetized using isoflurane inhalation, and a 100-μL phosphate-buffered saline solution containing ^{68}Ga-DOTA-SFLAP3 (HNO97, 37.9 MBq; HNO399, 26 MBq; HNO223, 27 MBq) or ^{68}Ga-DOTA-SFITGv6 (HNO97, 30 MBq; HNO399, 34 MBq; HNO223, 34 MBq) was injected into the tail vein. Three-dimensional PET images were captured (Siemens Inveon PET scanner) as previously described (*12*). To assess the biodistribution, 100 μL of a 20 nM ^{177}Lu-DOTA-SFLAP3 or ^{177}Lu-DOTA-SFITGv6 solution (1 MBq) were administered as a bolus injection into the tail vein. At each time point (30, 60, 120, 240, 360 min), we sacrificed 3 animals, collected peripheral blood and the respective organs, weighed the tissues, and measured the radioactivity using a γ-counter. Radioactivity (MBq) was expressed as percentage of injected dose (%ID) per gram of tissue.

Peptide Staining

Histochemical staining was performed using biotinylated polyethylene glycol 12–labeled peptides on acetone-fixed cryosections (5 μm) derived from snap-frozen HNSCC tissues as described previously (*12*). Briefly, to prevent background staining, HNSCC cryosections were preincubated with an SP-2001 avidin/biotin blocking kit (Vector Laboratories), and 10^{-5} M peptide diluted in Dako Antibody Diluent (Agilent) was subsequently applied at 4°C overnight. Detection of bound peptide was assessed using the Vectastain Elite ABC Kit (PK-6100; Vector Laboratories) according to the manufacturer's instructions. Peptide-binding specificity was ensured by using a peptide containing a scrambled (GRD) sequence and by incubation without peptide. Because of the instability of the peptide binding, staining was assessed on the same day as the binding experiment.

PET/CT Scanning of HNSCC Tumor Patient

An unenhanced PET/CT scan of a patient was obtained 60 and 180 min after intravenous injection of the ^{68}Ga-DOTA–labeled peptide using a Biograph mCt Flow PET/CT scanner (Siemens Medical Solution) and the following parameters: slice thickness of 5 mm, increment of 3–4 mm, soft-tissue reconstruction kernel, and CARE Dose4D (Siemens). Immediately after CT scanning, a whole-body PET scan was acquired in 3 dimensions (matrix, 200 × 200) using FlowMotion continuous-bed-motion technology (Siemens) at 0.7 cm/min. The emission data were corrected for randoms, scatter, and decay. Images were reconstructed using ordered-subsets expectation maximization with 2 iterations and 21 subsets and were Gauss-filtered to a transaxial resolution of 5 mm in full width at half maximum. Attenuation correction was performed using the low-dose unenhanced CT data. Uptake was quantitatively assessed using a region-of-interest technique and SUVs.

RESULTS

Binding of SFTI1 Derivates to $\alpha_v\beta_6$ Integrin–Expressing HNSCC Cell Lines

RGD motif–containing octamers of the natural $\alpha_v\beta_6$ integrin ligands fibronectin, tenascin C, vitronectin, LAP1, and LAP3 (Supplemental Table 1; supplemental materials are available at http://jnm.snmjournals.org) were grafted between Thr4 and Cys11 into the binding loop of the SFTI1 scaffold. First, the binding properties of ^{125}I-labeled SFFN1, SFTNC, SFVTN, SFLAP1 SFLAP3, and SFITGv6 were compared using 5 HNSCC cell lines differing in their $\alpha_v\beta_6$ integrin expression as assessed by flow cytometry

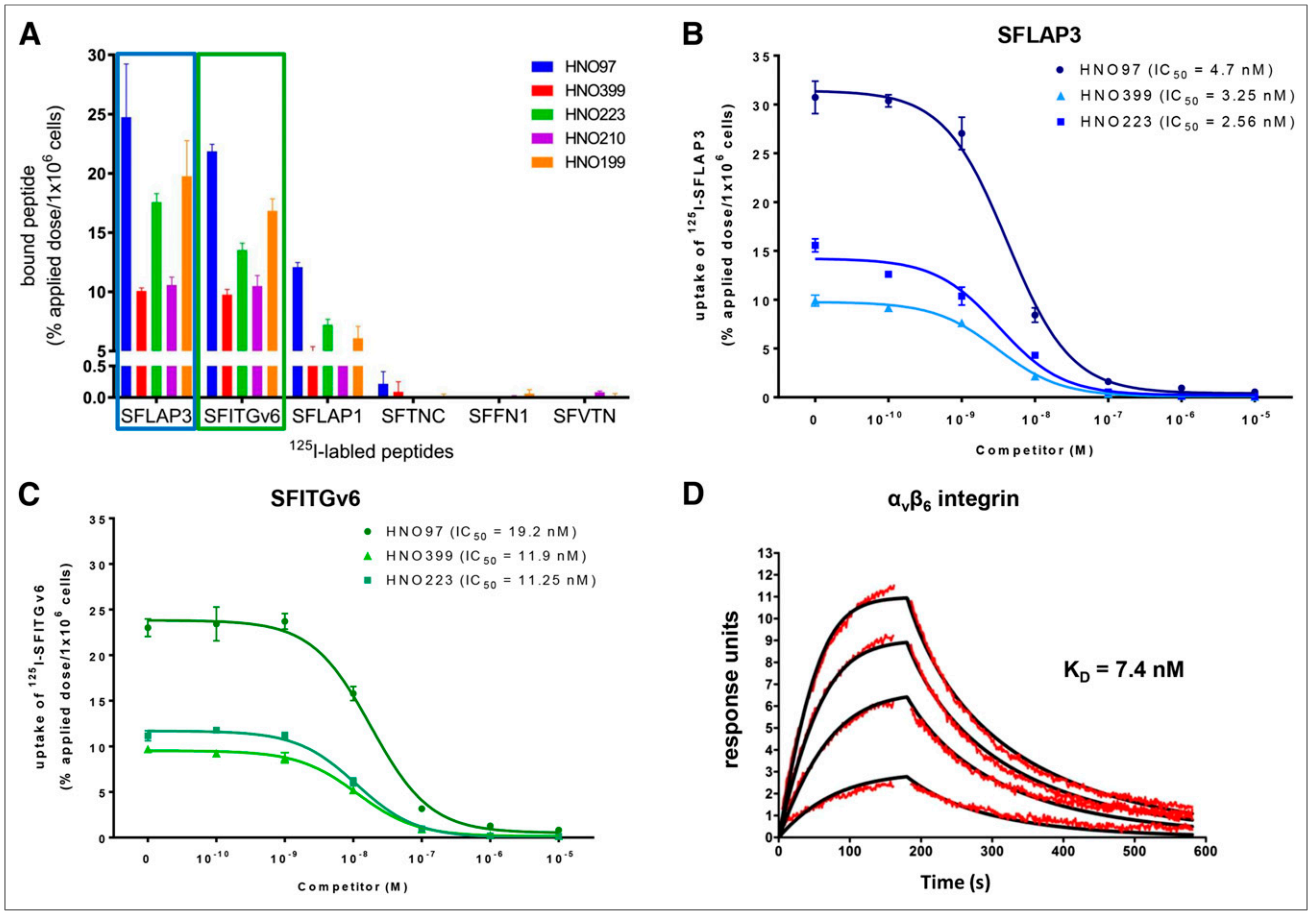

FIGURE 1. (A) Binding of ^{125}I-labeled SFLAP3, SFITGv6, SFLAP1, SFTNC, SFFN1, and SFVTN to different HNSCC cells after exposure to peptides for 60 min. Bars represent %AD/10^6 cells (HNO97, HNO399, HNO223, HNO210, and HNO199). Increasing concentrations (10^{-5}–10^{-10} M) of respective unlabeled peptide were used to compete for binding of ^{125}I-labeled SFLAP (B) and SFITGv6 (C) to HNSCC cell lines HNO97, HNO399, and HNO223 (%AD/10^6 cells). Data are mean and SD of triplicate measurements from representative experiment. (D) Affinity of $\alpha_v\beta_6$ integrin (applied concentrations: 1, 2, 3, and 4 μg/mL) for immobilized SFLAP3 (loading level: 12 response units) was measured by surface plasmon resonance assay (n = 3) with flow rate of 30 mL/min. Surface plasmon resonance sensograms were evaluated with BiaCore evaluation software (black curves) and correspond to experimentally fitted red curves. K_D was determined by 1:1 Langmuir model fit of surface plasmon resonance sensograms. IC_{50} = half-maximal inhibitory concentration.

(Supplemental Fig. 1). As shown in Figure 1A, ^{125}I-SFLAP3 displayed the highest binding capacity to all tested HNSCC cell lines (HNO97, 24.7%; HNO399, 10.1%; HNO199, 19.7%; HNO223, 17.6%; HNO210, 10.6%)—higher even than that of ^{125}I-SFITGv6 (HNO97, 21.8%; HNO399, 9.8%; HNO199, 16.8%; HNO223, 13.5%; HNO210, 10.5%). In contrast, only a moderate binding capacity was detected for SFLAP1 (4.1%–12.1%) and almost none (<1%) for SFFN1, SFTNC, and SFVTN (Fig. 1A). In summary, SFLAP3 and SFITGv6 demonstrated the highest binding capacity and, thus, were further investigated comparatively.

SFLAP3 Affinity for $\alpha_v\beta_6$ Integrin and Serum Stability

To assess the specificity of the peptide, binding competition experiments were performed. In all HNSCC cell lines, binding of ^{125}I-SFLAP3 and ^{125}I-SFITGv6 could almost be completely inhibited by adding 10^{-6} M unlabeled counterparts as competitor (Figs. 1B and 1C). However, SFLAP3 exhibited higher affinity than SFITGv6 (mean half-maximal inhibitory concentrations, 3.5 and 14.11 nM, respectively). Concordantly, the surface plasmon resonance assay revealed that SFLAP3 had a higher affinity than SFITGv6 for $\alpha_v\beta_6$ integrin (K_D = 7.4 and 14.8 nM, respectively) (Fig. 1D) (12). In contrast, SFLAP3 had a 10-fold lower affinity to $\alpha_v\beta_3$ integrin (K_D = 167 nM) (Supplemental Fig. 2A), further ensuring the $\alpha_v\beta_6$ integrin specificity of SFLAP3. Additionally, SFLAP3 showed high proteolytic stability, with no degradation over 24 h (Supplemental Fig. 2B), demonstrating suitability for in vivo applications.

Comparative Evaluation of Kinetics, Internalization, and Efflux

Considering time-dependent deionization of ^{125}I, the determination of kinetics, internalization, and efflux was performed using ^{177}Lu-DOTA–labeled peptides. Kinetic experiments revealed a continuous increase in peptide uptake over the whole period of measurement for both peptides. Yet, ^{177}Lu-DOTA-SFLAP3 exhibited a lower maximum binding capacity (HNO97, 18.5%; HNO223, 9.66%; HNO399, 4.31%) (Supplemental Fig. 3A) than ^{177}Lu-DOTA-SFITGv6 (HNO97, 22.15%; HNO223, 14.45%; HNO399, 5.85%) (Supplemental Fig. 3B). Accordingly, within 60 min after exposure to HNO97, we measured an increase in ^{177}Lu-DOTA-SFITGv6 binding of up to 16.85% and a fast internalization of up to 70% of the total bound peptide (Fig. 2B), but up to 11.14% binding and 60% internalization of ^{177}Lu-DOTA-SFLAP3

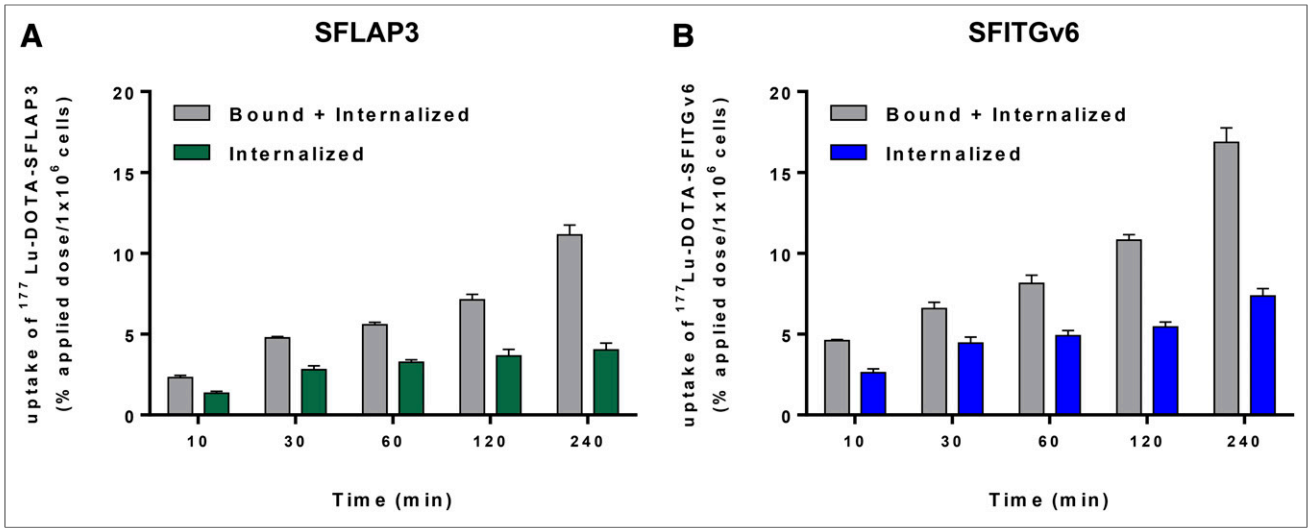

FIGURE 2. Uptake (gray bars) and internalization of ^{177}Lu-DOTA–labeled SFLAP3 (A) and SFITGv6 (B) in HNO97 cells. After incubation for 10, 30, 60, 120, and 240 min, radioactivity in lysates was determined and calculated as %AD/10^6 cells. Data are mean and SD of triplicate measurements from representative experiment.

(Fig. 2A). For both peptides, similar trends regarding a time-dependent increase in peptide binding and internalization were observed after exposure to HNO399 (Supplemental Figs. 4A and 4B) and HNO223 (Supplemental Figs. 4C and 4D), although the amount of internalized peptide slightly decreased (>45%). Concordantly, an efflux of more than 50% of the originally accumulated SFLAP3 and SFITGv6 within 120 min after termination of the uptake was measured (Figs. 3A and 3B). Notably, for ^{177}Lu-DOTA-SFLAP3, we observed a moderate renewed increase in binding and internalization after 240 min (Fig. 3A), possibly indicating peptide reuptake from the culture medium.

In Vivo Targeting Properties of SFLAP3 and SFITGv6

To compare the in vivo targeting properties of the peptides, small-animal PET imaging of HNO97, HNO399, and HNO223 xenografts was performed using ^{68}Ga-DOTA–labeled SFLAP3 and SFITGv6 as radiotracer. In HNO97 tumor lesions, a fast and continuous accumulation of ^{68}Ga-DOTA-SFLAP3 (SUV_{mean}, 0.63) (Fig. 4A; Supplemental Fig. 5A) and ^{68}Ga-DOTA-SFITGv6 (SUV_{mean}, 0.68) (Supplemental Figs. 5B and 5C) was measured within 60 min after injection and stayed for at least 140 min (Supplemental Figs. 5D and 5E). Nonspecific peptide activity cleared quickly from the blood, resulting in images with excellent tumor-to-background ratios. Accordingly, the biodistribution of ^{177}Lu-DOTA-SFLAP3 in tumor lesions and individual organs of HNO97 xenografts revealed maximal peptide accumulation in the tumors after 60 min (9.1 ± 1.2 %ID/g), followed by a decrease to 5.80 ± 1.44 %ID/g at 360 min after injection (Fig. 4B). In contrast, the maximal uptake of ^{177}Lu-DOTA-SFITGv6 in HNO97 tumors (6.73 ± 1.00 %ID/g) was already present at 30 min after injection, and uptake decreased to 2.43 ± 0.51 %ID/g after 360 min (Supplemental Fig. 5F). Small-animal PET imaging of HNO399 (Fig. 4C; Supplemental Fig. 6B) and HNO223 xenografts (Supplemental Figs. 7A and 7B) revealed less accumulation of ^{68}Ga-DOTA-SFLAP3 (SUV_{mean}, 0.44 for

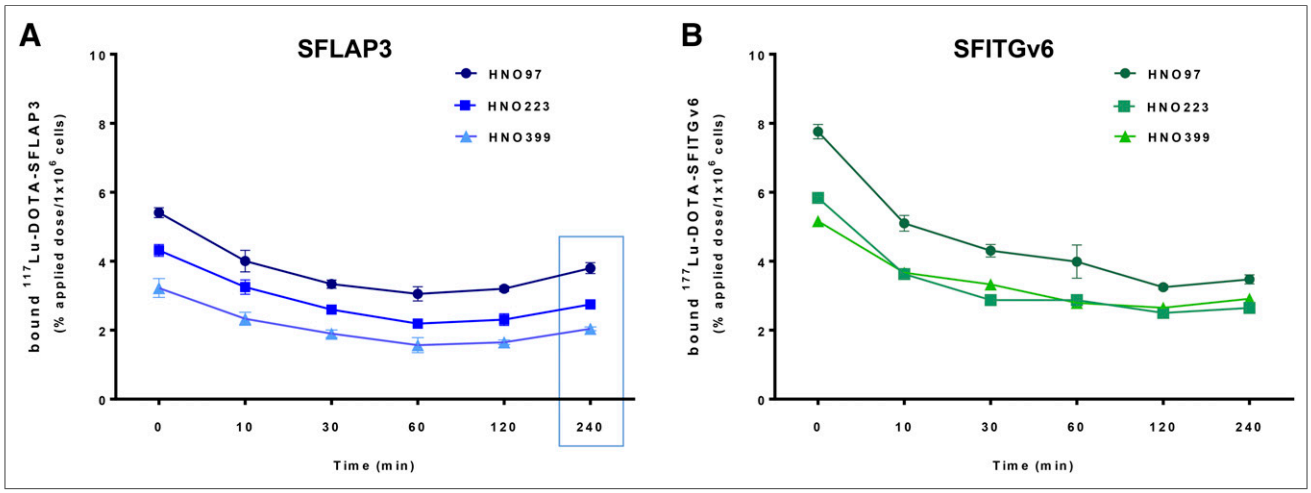

FIGURE 3. Time-dependent efflux of SFLAP3 (A) and SFITGv6 (B) from HNSCC cell lines. HNO97, HNO399, and HNO223 cells were exposed to ^{177}Lu-DOTA–labeled peptides for 60 min. After replacement of culture medium, radioactivity in cell lysates was measured immediately and after 10, 30, 60, 120, and 240 min and calculated as %AD/10^6 cells. Data are mean and SD of triplicate measurements from representative experiment.

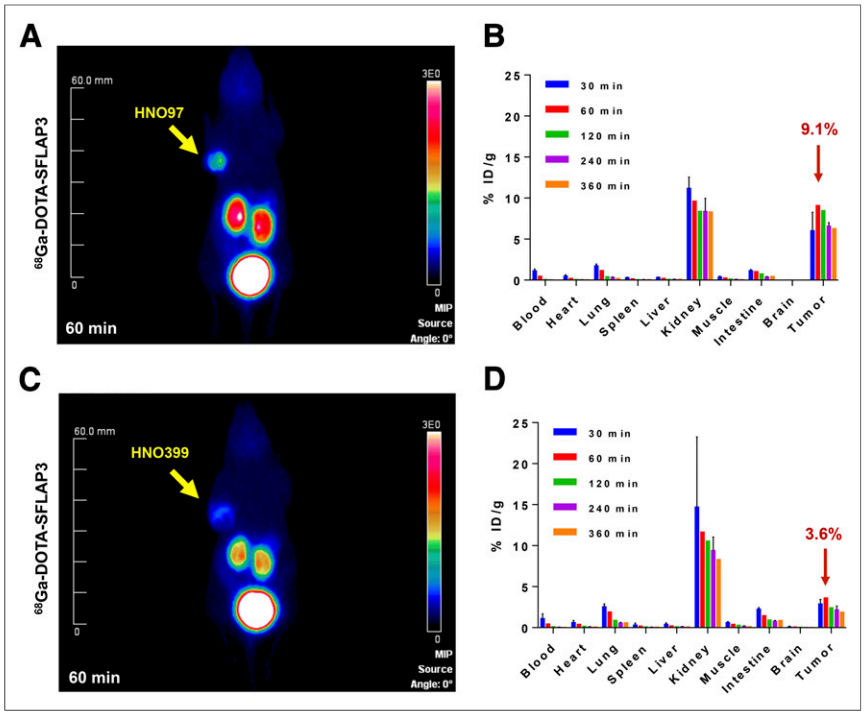

FIGURE 4. Small-animal PET imaging of mice bearing HNO97 (A) and HNO399 (C) xenografts 60 min after injection of ^{68}Ga-DOTA-SFLAP3. Biodistribution of ^{177}LU-DOTA-SFLAP3 in tumor and organs of HNO97 (B) and HNO399 (D) tumor–bearing mice was measured 30, 60, 120, 240, and 360 min after injection and calculated as %ID/g. Data are mean of 3 per time point and SD. MIP = maximum-intensity projection.

HNO399 and 0.32 for HNO223) (Supplemental Figs. 6A and 7C) and of ^{68}Ga-DOTA-SFITGv6 (SUV_{mean}, 0.33 for HNO399 and 0.23 for HNO223) (Supplemental Figs. 6C and 7D). Accordingly, we measured a maximal ^{177}Lu-DOTA-SFLAP3 accumulation of 3.6 % ID/g (Fig. 4D) and 3.4 %ID/g (Supplemental Fig. 7E) in HNO399 and HNO233 xenografts, respectively, at 60 min after injection, followed by a decrease to almost 2% at 360 min. Less than 1 %ID/g was detected in the blood and most tissues of xenograft mice 120 min after injection of either peptide, accounting for tumor-to-tissue ratios predominantly above 1 (Supplemental Tables 2A–2D). However, in the kidneys we observed a constant high SFLAP3 retention (8–14 % ID/g), which was indeed clearly reduced in comparison to SFITGv6 (Supplemental Fig. 5F).

In Situ Binding Properties of SFLAP3

In analogy to the previous experiments (*12*), we compared the binding specificity of the peptides to sections of HNO97 xenografts and patient-derived HNO399 and HNO210 tumors by peptide histochemical staining using biotin-labeled SFLAP3 and SFITGv6. Although SFLAP3 showed a slightly fainter staining, both peptides revealed tumor cell–specific binding, whereas lower peptide binding was observed at the stromal compartments (Fig. 5). In contrast, no binding of the GRD sequence containing peptide was observed, further corroborating the specificity of the SFLAP3 peptide.

SFLAP3 Accumulation in HNSCC Lesions and Lymph Node Metastases

Finally, we investigated the therapeutic or diagnostic suitability of SFLAP3, using the example of a 79-y-old male carcinoma patient who presented with lymph node swelling in the right cervical area, assuming the diagnosis cancer of unknown primary. To clarify the diagnosis, 322 MBq of ^{68}Ga-DOTA–labeled SFLAP3 were administered and PET/CT performed. After 60 min, we observed a tumor-specific accumulation of SFLAP3 at the primary tumor lesion (right site of aryepiglottic folds; median SUV_{max}, 5.1) (Fig. 6) and at the right cervical area (SUV_{max}, 4.1) (Supplemental Table 3). The histopathologic examination of the surgically resected respective tissues proved the presence of level II/III squamous cell carcinoma and corresponding lymph node metastases at the respective locations. The correlation of PET findings and histopathologic findings revealed the primary tumor lesion to be subepithelial connective tissue infiltrated by moderately differentiated squamous cell carcinoma (Fig. 6C). The tumor lesion at the right cervical area was classified as cyst wall and content; histopathologic analysis showed infiltrates of an epithelial neoplasia with a solid growth pattern (Fig. 6B). Moderate tracer accumulation was also seen in a lymph node in the right cervical area (SUV_{max}, 2.2), which was histopathologically classified as a lymph node infiltrated by epithelial tumor cells and neoplasia with a solid growth pattern (Fig. 6D).

DISCUSSION

SFTI1 has already been proven to be a suitable scaffold for the development of extremely stable peptides targeting tumor-associated receptors, including the $\alpha_v\beta_6$ integrin–specific peptide SFITGv6 (12,20). $\alpha_v\beta_6$ integrin has been shown to be expressed in up to 99.9% of HNSCC (9,14), as well as in lung (4), colon (7), breast (21), and pancreas carcinoma (6), and is often associated with a poor prognosis (9). Thus, $\alpha_v\beta_6$ integrin represents an important target for imaging and therapy for a variety of epithelial malignancies (22–25). To design novel target-specific peptides, we introduced the RGD-containing octamer of natural $\alpha_v\beta_6$ integrin ligands resembling the RGDLXXL sequence into the SFTI1 scaffold and compared the specificity and affinity of the novel peptides with that of SFITGv6.

In comparing the binding properties of these SFTI1 derivates, we identified the superiority of the $\alpha_v\beta_6$ integrin–specific peptide SFLAP3, containing the amino acid sequence GRGDLGRL. Comparative analysis of SFLAP3 and SFITGv6 revealed improved binding (>20%) of the novel peptide to several HNSCC cell lines corresponding to their $\alpha_v\beta_6$ integrin expression profile. Considering the importance of the RGDLXXL motif—in particular, the DLXXL sequence—for $\alpha_v\beta_6$ integrin binding affinity and specificity (26–28), it is not surprising that SFLAP3 provides significant binding properties. In contrast, for SFLAP1, SFFN1, SFVTN, and SFTNC—partially or completely lacking the LXXL motif—we observed less or even almost no binding. Although being physiologically involved in $\alpha_v\beta_6$ integrin–dependent promotion of migration, invasion, and signal transduction pathways (14), the RGD motif–containing sequences of

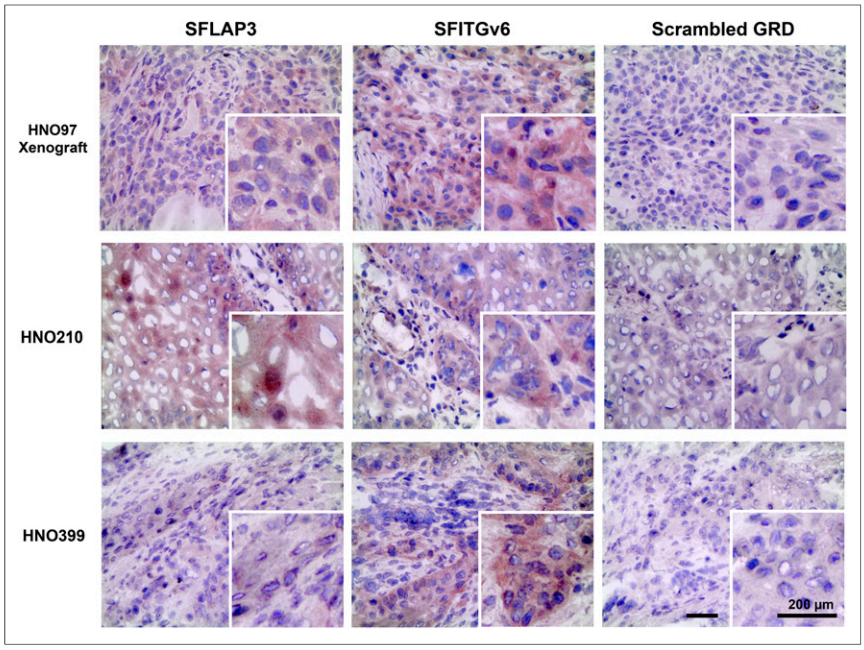

FIGURE 5. Histochemical peptide staining of HNSCC cyrosections of HNO97 xenografts and of patient-derived HNO399 and HNO210 tumor sections performed with 10^{-5} M biotinylated polyethylene glycol 12–labeled SFLAP3 and SFITGv6. As control, scrambled SFLAP3 derivate containing GRD was applied. Scale bar = 50 µm.

LAP1, fibronectin, vitronectin, and tenascin C incorporated into the SFTI1 scaffold might not allow for $\alpha_v\beta_6$ integrin affinity and specificity in vitro.

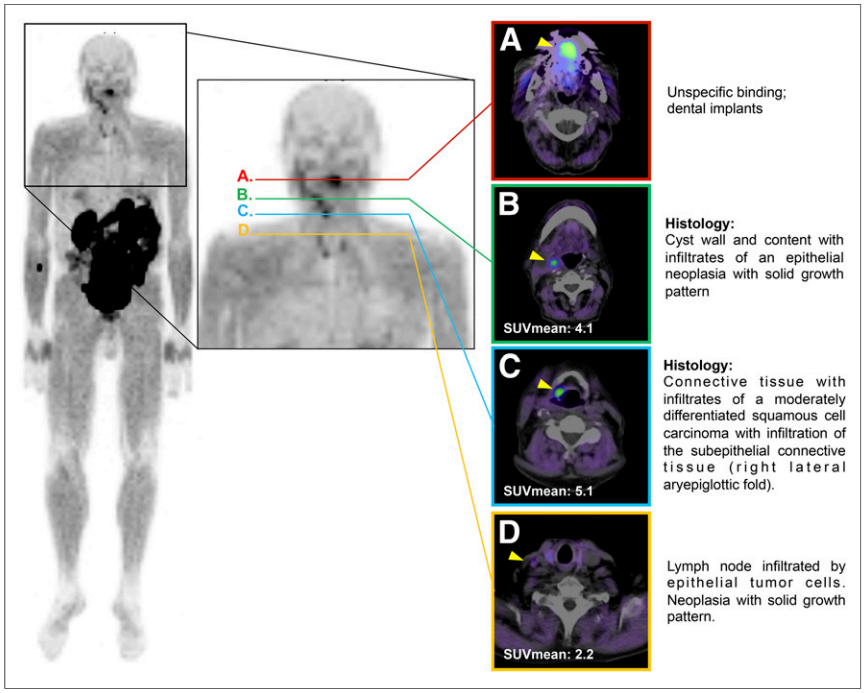

FIGURE 6. Transaxial PET/CT scans of HNSCC tumor patient after application of 322 MBq of ^{68}Ga-DOTA-SFLAP3, with arrowheads indicating peptide accumulation. (A) Level showing unspecific binding. (B) Level showing cyst wall and content. (C) Level showing primary tumor. (D) Level showing lymph node infiltration.

As expected from stability analysis of the naturally occurring SFTI1 (13) and the SFTI1 derivates DLL4 (20) and SFITGv6 (12), SFLAP3 also demonstrated marked stability in human serum over 24 h. Additionally, an improved affinity of SFLAP3 (K_D = 7.4 nM) for $\alpha_v\beta_6$ integrin when compared with SFITGv6 was measured. Subsequent investigation of ^{177}Lu-DOTA–labeled SFLAP3 and SFITGv6 regarding kinetics, internalization, and efflux revealed a continuous increase in SFLAP3 binding (≤18.5% within 240 min) and fast internalization (>60%) followed by a decrease (<50%). Correspondingly, we observed greater than 50% efflux and almost 50% retention of the originally accumulated peptide over 120 min, justifying further in vivo evaluation. These experiments also demonstrated a consistently higher binding (≤5.7%) of ^{177}Lu-DOTA–labeled SFITGv6 than of SFLAP3. It is thought that the chemical properties of the SFLAP3 and SFITGv6 amino acid composition influence the binding capacity of DOTA–labeled peptides differently.

On the basis of the excellent tumor-to-background ratios, we were able to selectively image HNSCC xenografts using small-animal PET at 60–140 min after the administration of ^{68}Ga-DOTA–labeled SFLAP3 and SFITGv6. Unbound and nonspecifically bound peptide rapidly cleared from the blood and the surrounding tissues, except for the kidneys. As expected from the $\alpha_v\beta_6$ integrin expression profile of HNSCC cell lines, we detected a rather low but clearly visible accumulation of both ^{68}Ga-DOTA-SFLAP3 (SUV_{mean}, 0.63) and ^{68}Ga-DOTA-SFITGv6 (SUV_{mean}, 0.68) in HNO97 xenografts. In contrast, HNO399 and HNO223 xenografts showed a lower uptake of the ^{68}Ga-DOTA–labeled peptides but a generally higher affinity of ^{68}Ga-DOTA-SFLAP3 (SUV_{mean}, 0.44; SUV, 0.32) than did ^{68}Ga-DOTA-SFITGv6 (SUV_{mean}, 0.32; SUV_{mean}, 0.23). The biodistribution of ^{177}Lu-DOTA–labeled peptides in HNSCC xenograft mice confirmed the improved affinity of SFLAP3 for $\alpha_v\beta_6$ integrin–expressing tumors. In HNO97 tumors, we found a marked accumulation of SFLAP3 (≤9.10 %ID/g) and SFITGv6 (6.73 %ID/g), compared with that in healthy tissues, even after 240 and 360 min. In contrast, less than 4 %ID/g of SFLAP3 was measured for HNO399 and HNO223, emphasizing the importance of pronounced target expression for selective in vivo tumor imaging and targeting. As expected from a previous biodistribution analysis of $\alpha_v\beta_6$ integrin binding peptides in HNO97 (12) and BxPC-3 xenografts (11), a remarkable but slightly decreasing

accumulation of ^{177}Lu-DOTA-SFLAP3 was noticed in the kidneys of HNSCC xenografts. Although the renal retention of SFLAP3 was clearly lower than that of SFITGv6, we can recommend that the pharmacokinetic properties of the peptide be improved.

Even though peptide-based histochemical staining revealed a moderate but tumor cell–specific binding of SFLAP3 to HNO97 xenografts and patient-derived HNSCC tumor cyrosections, the ^{68}Ga-DOTA–labeled peptide was successfully used as a radiotracer for PET/CT imaging of a patient with a carcinoma of unknown primary, leading to the discovery of a histologically proven HNSCC and a corresponding lymph node metastasis. In line with the small-animal PET imaging results for HNSCC xenografts, the SUVs in the patient persisted from 60 min (SUV_{max}, 5.1) to 180 min (SUV_{max}, 4.6) after injection, demonstrating the diagnostic suitability of the peptide.

In analogy to the ^{68}Ga-DOTA-SFITGv6 PET/CT findings for patients with HNSCC and non–small cell lung carcinoma (12), ^{68}Ga-DOTA-SFLAP3 PET/CT revealed peptide accumulation in the kidneys, secretion into the gastrointestinal tract, and intraluminal transport to the terminal ileum and the cecum. Thus, when SFLAP3 is being considered for imaging of $\alpha_v\beta_6$ integrin–positive carcinomas occurring below the diaphragm, administration of laxatives (reducing intrabowel activity and avoiding a high background signal) and improvement of the pharmacokinetic properties of the peptide are required.

CONCLUSION

We found that the $\alpha_v\beta_6$ integrin–binding peptide SFLAP3 provides improved affinity and excellent binding properties for $\alpha_v\beta_6$ integrin–expressing HNSCC tumors in vitro and in vivo. Thus, SFLAP3 represents a promising tracer for both diagnostic imaging and targeted therapy of $\alpha_v\beta_6$ integrin–expressing tumors.

DISCLOSURE

This project was supported by the Deutsche Forschungsgemeinschaft (DFG) (HA 2901/12-1). No other potential conflict of interest relevant to this article was reported.

ACKNOWLEDGMENTS

We thank Vanessa Kohl and Marlene Tesch for providing technical assistance, Ursula Schierbaum and Karin Leotta for performing animal experiments, Dr. Esther Herpel (Tissue Bank, National Center for Tumor Diseases (NCT), Heidelberg, Germany) for examining the tumor tissues histopathologically, and Dr. Carmen Rapp for proofreading the manuscript.

REFERENCES

1. Zhang Y, Wang H. Integrin signalling and function in immune cells. *Immunology.* 2012;135:268–275.
2. Seguin L, Desgrosellier JS, Weis SM, Cheresh DA. Integrins and cancer: regulators of cancer stemness, metastasis, and drug resistance. *Trends Cell Biol.* 2015;25:234–240.
3. Desgrosellier JS, Cheresh DA. Integrins in cancer: biological implications and therapeutic opportunities. *Nat Rev Cancer.* 2010;10:9–22.
4. Elayadi AN, Samli KN, Prudkin L, et al. A peptide selected by biopanning identifies the integrin αvβ6 as prognostic biomarker for nonsmall cell lung cancer. *Cancer Res.* 2007;67:5889–5895.
5. Ahmed N, Riley C, Rice GE, Quinn MA, Baker MS. $\alpha_v\beta_6$ integrin-A marker for the malignant potential of epithelial ovarian cancer. *J Histochem Cytochem.* 2002;50:1371–1380.
6. Sipos B, Hahn D, Carceller A, et al. Immunohistochemical screening for β6-integrin subunit expression in adenocarcinomas using a novel monoclonal antibody reveals strong up-regulation in pancreatic ductal adenocarcinomas *in vivo* and *in vitro*. *Histopathology.* 2004;45:226–236.
7. Bates RC, Bellovin DI, Brown C, et al. Transcriptional activation of integrin β6 during the epithelial-mesenchymal transition defines a novel prognostic indicator of aggressive colon carcinoma. *J Clin Invest.* 2005;115:339–347.
8. Hazelbag S, Kenter GG, Gorter A, et al. Overexpression of the alpha v beta 6 integrin in cervical squamous cell carcinoma is a prognostic factor for decreased survival. *J Pathol.* 2007;212:316–324.
9. Bandyopadhyay A, Raghavan S. Defining the role of integrin alphavbeta6 in cancer. *Curr Drug Targets.* 2009;10:645–652.
10. Hackel BJ, Kimura RH, Miao Z, et al. ^{18}F-fluorobenzoate-labeled cystine knot peptides for PET imaging of integrin αvβ6. *J Nucl Med.* 2013;54:1101–1105.
11. Hausner SH, Abbey CK, Bold RJ, et al. Targeted in vivo imaging of integrin avb6 with an improved radiotracer and its relevance in a pancreatic tumor model. *Cancer Res.* 2009;69:5843–5850.
12. Altmann A, Sauter M, Roesch S, et al. Identification of a novel ITGαvβ6-binding peptide using protein separation and phage display. *Clin Cancer Res.* 2017;23:4170–4180.
13. Boy RG, Mier W, Nothelfer EM, et al. Sunflower trypsin inhibitor 1 derivatives as molecular scaffolds for the development of novel peptidic radiopharmaceuticals. *Mol Imaging Biol.* 2010;12:377–385.
14. Thomas GJ, Nyström ML, Marshall JF. Alphavbeta6 integrin in wound healing and cancer of the oral cavity. *J Oral Pathol Med.* 2006;35:1–10.
15. Annes JP, Rifkin DB, Munger JS. The integrin alphaVbeta6 binds and activates latent TGFbeta3. *FEBS Lett.* 2002;511:65–68.
16. Zavadil J, Böttinger EP. TGF-beta and epithelial-to-mesenchymal transitions. *Oncogene.* 2005;24:5764–5774.
17. Annes JP, Chen Y, Munger JS, Rifkin DB. Integrin αVβ6-mediated activation of latent TGF-β requires the latent TGF-β binding protein-1. *J Cell Biol.* 2004;165:723–734.
18. Wipff P-J, Hinz B. Integrins and the activation of latent transforming growth factor beta1: an intimate relationship. *Eur J Cell Biol.* 2008;87:601–615.
19. Ninck S, Reisser C, Dyckhoff G, Helmke B, Bauer H, Herold-Mende C. Expression profiles of angiogenic growth factors in squamous cell carcinomas of the head and neck. *Int J Cancer.* 2003;106:34–44.
20. Zoller F, Markert A, Barthe P, et al. Combination of phage display and molecular grafting generates highly specific tumor-targeting miniproteins. *Angew Chem Int Ed Engl.* 2012;51:13136–13139.
21. Arihiro K, Kaneko M, Fujii S, Inai K, Yokosaki Y. Significance of alpha 9 beta 1 and alpha v beta 6 integrin expression in breast carcinoma. *Breast Cancer.* 2000;7:19–26.
22. Saha A, Ellison D, Thomas GJ, et al. High-resolution in vivo imaging of breast cancer by targeting the pro-invasive integrin alphavbeta6. *J Pathol.* 2010;222:52–63.
23. Hausner SH, Bauer N, Hu LY, Knight LM, Sutcliffe JL. The effect of bi-terminal PEGylation of an integrin $\alpha v\beta_6$-targeted ^{18}F peptide on pharmacokinetics and tumor uptake. *J Nucl Med.* 2015;56:784–790.
24. Zhu X, Li J, Hong Y, et al. ^{99m}Tc-labeled cystine knot peptide targeting integrin αvβ6 for tumor SPECT imaging. *Mol Pharm.* 2014;11:1208–1217.
25. Kimura RH, Teed R, Hackel BJ, et al. Pharmacokinetically stabilized cystine knot peptides that bind alpha-v-beta-6 integrin with single-digit nanomolar affinities for detection of pancreatic cancer. *Clin Cancer Res.* 2012;18:839–849.
26. Kraft S, Diefenbach B, Mehta R, Jonczyk A, Luckenbach GA, Goodman SL. Definition of an unexpected ligand recognition motif for alphav beta6 integrin. *J Biol Chem.* 1999;274:1979–1985.
27. DiCara D, Rapisarda C, Sutcliffe JL, et al. Structure-function analysis of Arg-Gly-Asp helix motifs in alpha v beta 6 integrin ligands. *J Biol Chem.* 2007;282:9657–9665.
28. Nothelfer E-M, Zitzmann-Kolbe S, Garcia-Boy R, et al. Identification and characterization of a peptide with affinity to head and neck cancer. *J Nucl Med.* 2009;50:426–434.